

High-speed dual color fluorescence lifetime endomicroscopy for highly-multiplexed pulmonary diagnostic applications and detection of labeled bacteria

ETTORE PEDRETTI^{1,7}, MICHAEL G. TANNER^{2,3}, TUSHAR R. CHOUDHARY^{1,3}, NIKOLA KRSTAJIĆ^{3,4,8}, ALICIA MEGIA-FERNANDEZ⁵, ROBERT K. HENDERSON⁴, MARK BRADLEY⁵, ROBERT R. THOMSON^{2,3}, JOHN M. GIRKIN⁶, KEV DHALIWAL³ AND PAUL A. DALGARNO^{1,*}

¹ Institute of Biological Chemistry, Biophysics and Bioengineering, School of Engineering and Physical Sciences, Heriot-Watt University, Edinburgh EH14 4AS, UK

² Scottish Universities Physics Alliance (SUPA), Institute of Photonics and Quantum Sciences, School of Engineering and Physical Sciences, Heriot-Watt University, Edinburgh EH14 4AS, UK

³ EPSRC IRC Hub, MRC Centre for Inflammation Research, Queen's Medical Research Centre, University of Edinburgh, Edinburgh EH16 4TJ, UK

⁴ Institute for Integrated Micro and Nano Systems, School of Engineering, University of Edinburgh, Edinburgh EH9 3FF, UK

⁵ EaStChem, School of Chemistry, University of Edinburgh, Edinburgh EH9 3FJ, UK

⁶ Department of Physics, University of Durham, Durham DH1 3LE, UK

⁷ Currently with the Leibniz-Institute für Astrophysik Potsdam, Deutschland

⁸ Currently with the University of Dundee, School of Science and Engineering, Dundee, United Kingdom
*P.A.Dalgarno@hw.ac.uk

Abstract: We present a dual color laser scanning endomicroscope capable of fluorescence lifetime endomicroscopy at one frame per second (FPS). The scanning system uses a coherent imaging fiber with 30,000 cores. High-speed lifetime imaging is achieved by distributing the signal over an array of 1024 parallel single-photon avalanche photo-diode detectors (SPADs), minimizing detection dead time maximizing the number of photons detected per excitation pulse without photon pile-up to achieve the high frame rate. Dual color fluorescence imaging is achieved by temporally shifting the dual excitation lasers, with respect to each other, to separate the two spectrally distinct fluorescent decays. Combining the temporal encoding, to provide spectral separation, with lifetime measurements we show a one FPS, multi-channel endomicroscopy platform for clinical applications and diagnosis. We demonstrate the potential of the system by imaging smartprobe-labeled bacteria in ex vivo samples of human lung using lifetime to differentiate bacterial fluorescence from the strong background lung auto-fluorescence which was used to provide structural information.

© 2018 Optical Society of America under the terms of the [OSA Open Access Publishing Agreement](#)

OCIS codes: (170.0170) Medical optics and biotechnology; (170.3890) Medical optics instrumentation; (180.0180) Microscopy; (170.2520) Fluorescence microscopy; (170.2150) Lifetime-based sensing (170.3650) Endoscopic imaging; (030.5260) Photon counting.

References and links

1. A. Osdoit, F. Lacombe, C. Cavé, S. Loiseau, and E. Peltier, "To see the unseeable: confocal miniprobes for routine microscopic imaging during endoscopy," in "Endoscopic Microscopy II," (Proc. SPIE 6432, 2007), p. 64320F.
2. O. Danilevskaya, A. Averyanov, N. Klimko, V. Lesnyak, A. Sorokina, D. Sazonov, and F. Zabolzaev, "The case of diagnostics of invasive pulmonary aspergillosis by in vivo probe-based confocal laser endomicroscopy of central and distal airways," *Medical mycology case reports* **5**, 35–39 (2014).

3. L. Thiberville, M. Salaün, S. Lachkar, S. Dominique, S. Moreno-Swirc, C. Vever-Bizet, and G. Bourg-Heckly, "Human in vivo fluorescence microimaging of the alveolar ducts and sacs during bronchoscopy," *European Respiratory Journal* **33**, 974–985 (2009).
4. Y. Sun, R. Liu, D. S. Elson, C. W. Hollars, J. A. Jo, J. Park, Y. Sun, and L. Marcu, "Simultaneous time-and wavelength-resolved fluorescence spectroscopy for near real-time tissue diagnosis," *Optics letters* **33**, 630–632 (2008).
5. N. Krstajić, A. R. Akram, T. R. Choudhary, N. McDonald, M. G. Tanner, E. Pedretti, P. A. Dalgarno, E. Scholefield, J. M. Girkin, A. Moore, M. Bradley, and K. Dhaliwal, "Two-color widefield fluorescence microendoscopy enables multiplexed molecular imaging in the alveolar space of human lung tissue," *Journal of Biomedical Optics* **21**, 046009 (2016).
6. A. R. Akram, S. V. Chankeshwara, E. Scholefield, T. Aslam, N. McDonald, A. Megia-Fernandez, A. Marshall, B. Mills, N. Avlonitis, T. H. Craven, A. M. Smyth, D. S. Collie, C. Gray, N. Hirani, A. T. Hill, J. R. Govan, T. Walsh, C. Haslett, M. Bradley, and K. Dhaliwal, "Immediate in situ identification of gram-negative bacteria in human lungs using a topical fluorescent peptide targeted against lipid a," *Science Translational Medicine* (In Press, 2018).
7. T. R. Choudhary, M. Bradley, R. R. Duncan, and K. Dhaliwal, "Towards in vivo bacterial detection in human lung (conference presentation)," in "Optical Techniques in Pulmonary Medicine II," (Proc. SPIE 10041, 2017), p. 100410M.
8. C. Stringari, A. Cinquin, O. Cinquin, M. A. Digman, P. J. Donovan, and E. Gratton, "Phasor approach to fluorescence lifetime microscopy distinguishes different metabolic states of germ cells in a live tissue," *Proceedings of the National Academy of Sciences* **108**, 13582–13587 (2011).
9. H. Wallrabe and A. Periasamy, "Imaging protein molecules using fret and flim microscopy," *Current opinion in biotechnology* **16**, 19–27 (2005).
10. Y. Sun, J. Phipps, D. S. Elson, H. Stoy, S. Tinling, J. Meier, B. Poirier, F. S. Chuang, D. G. Farwell, and L. Marcu, "Fluorescence lifetime imaging microscopy: in vivo application to diagnosis of oral carcinoma," *Optics letters* **34**, 2081–2083 (2009).
11. G. Kennedy, H. Manning, D. Elson, M. Neil, G. Stamp, B. Viellerobe, F. Lacombe, C. Dunsby, and P. French, "A fluorescence lifetime imaging scanning confocal endomicroscope," *Journal of Biophotonics* **3**, 103–107 (2010).
12. J. Bec, H. Xie, D. R. Yankelevich, F. Zhou, Y. Sun, N. Ghata, R. Aldredge, and L. Marcu, "Design, construction, and validation of a rotary multifunctional intravascular diagnostic catheter combining multispectral fluorescence lifetime imaging and intravascular ultrasound," *Journal of biomedical optics* **17**, 1060121–10601210 (2012).
13. D. R. Yankelevich, D. Ma, J. Liu, Y. Sun, Y. Sun, J. Bec, D. S. Elson, and L. Marcu, "Design and evaluation of a device for fast multispectral time-resolved fluorescence spectroscopy and imaging," *Review of Scientific Instruments* **85**, 034303 (2014).
14. E. Gratton, S. Breusegem, J. D. Sutin, Q. Ruan, and N. P. Barry, "Fluorescence lifetime imaging for the two-photon microscope: time-domain and frequency-domain methods," *Journal of biomedical optics* **8**, 381–391 (2003).
15. S. Poland, A. Erdogan, N. Krstajic, J. Levitt, V. Devauges, R. Walker, D. Li, S. Ameer-Beg, and R. Henderson, "A new high-speed centre of mass method incorporating background subtraction for accurate determination of fluorescence lifetime," *Optics Express* **24**, 6899–6915 (2016).
16. J. Richardson, R. Walker, L. Grant, D. Stoppa, F. Borghetti, E. Charbon, M. Gersbach, and R. K. Henderson, "A 32× 32 50ps resolution 10 bit time to digital converter array in 130nm cmos for time correlated imaging," in "Custom Integrated Circuits Conference, 2009. CICC'09. IEEE," (IEEE, 2009), pp. 77–80.
17. N. Krstajić, S. Poland, J. Levitt, R. Walker, A. Erdogan, S. Ameer-Beg, and R. K. Henderson, "0.5 billion events per second time correlated single photon counting using cmos spad arrays," *Opt. Lett.* **40**, 4305–4308 (2015).
18. A. Perperidis, H. E. Parker, A. Karam-Eldaly, Y. Altmann, K. Dhaliwal, R. R. Thomson, M. G. Tanner, and S. McLaughlin, "Characterization and modelling of inter-core coupling in coherent fiber bundles," *Opt. Express* **25**, 11932–11953 (2017).
19. F. Ceccarelli, A. Gulinatti, I. Labanca, I. Rech, and M. Ghioni, "Development and characterization of an 8x8 spad-array module for gigacount per second applications," in "Photon Counting Applications 2017," (Proc. SPIE 10229, 2017), p. 102290E.
20. W. Becker, *Advanced time-correlated single photon counting techniques*, vol. 81 (Springer Science & Business Media, 2005).
21. D. C. Wells, E. W. Greisen, and R. H. Harten, "FITS - a Flexible Image Transport System," *A&AS* **44**, 363 (1981).
22. E. Jones, T. Oliphant, and P. Peterson, "{SciPy}: open source scientific tools for {Python}," (2014).
23. T. R. Choudhary, M. G. Tanner, A. Megia-Fernandez, K. Harrington, H. A. Wood, S. Chankeshwara, P. Zhu, D. Choudhury, F. Yu, R. R. Thomson, R. R. Duncan, K. Dhaliwal, and M. Bradley, "Multiplexed fibre optic sensing in the distal lung (conference presentation)," in "Optical Fibers and Sensors for Medical Diagnostics and Treatment Applications XVII," (Proc. SPIE 10058, 2017), p. 100580E.
24. T. R. Choudhary, M. G. Tanner, A. Megia-Fernandez, K. Harrington, H. A. Wood, A. Marshall, P. Zhu, S. Chankeshwara, D. Choudhury, G. Monro, M. Ucuncu, F. Yu, R. R. Duncan, R. R. Thomson, K. Dhaliwal, and M. Bradley, "High fidelity fibre-based physiological sensing deep in tissue (in review)," *Scientific Reports* (2018).
25. F. Pérez and B. E. Granger, "IPython: a system for interactive scientific computing," *Computing in Science and Engineering* **9**, 21–29 (2007).
26. J. D. Hunter, "Matplotlib: A 2d graphics environment," *Computing In Science & Engineering* **9**, 90–95 (2007).
27. S. Behnel, R. Bradshaw, C. Citro, L. Dalcin, D. S. Seljebotn, and K. Smith, "Cython: The best of both worlds,"

1. Introduction

Probe-based confocal laser endomicroscopy (pCLE) is a minimally invasive technique used in pulmonary medicine to access the alveolar space [1]. Typically, pCLE takes advantage of the auto-fluorescence from the elastin, collagen, porphyrins, flavin adenine dinucleotide (FAD) and nicotinamide adenine dinucleotide (NADH) present in the lung to provide high contrast, in-situ cellular and sub-cellular-level images of the lung [1]. Such approaches have been hugely successful for pulmonary medicine and there are a number of commercial systems available for clinical use [1]. Examples of clinical applications include invasive pulmonary aspergillosis (IPA) that can be detected by monitoring morphological changes in the alveolar elastin networks [2] and the study of macrophage activity [3]. However, despite the success and impact of such systems, relying solely on auto-fluorescence is limiting. Primarily it restricts the ability to identify and distinguish from nearby tissues the specific bacterial colonies that would provide crucial clinical information for diagnosis and treatment.

Currently the most robust solution to identify bacterial colonies is to tag bacteria with fluorescent labels so that during imaging they are spectrally distinct from the inherent background auto-fluorescence. Instruments capable of such multi-wavelength endoscopic imaging [4] have been commercially available for some time. We have previously demonstrated a novel multi-channel fluorescence platform designed specifically for endomicroscopy for pulmonary medicine [5]. Furthermore, we have also developed selective bacterial fluorescent probes that enable detection and differentiation of bacteria in the human lung [6, 7]. However, fluorescence endomicroscopy, like all fluorescence imaging modalities, is typically limited to 2 or 3 channels, restricted by spectral mixing that enforces tight bandwidth, filtering and imaging constraints. These challenges are exacerbated in the pulmonary system due to the high intensity green background autofluorescence.

Fluorescence lifetime imaging (FLIM) is an alternative, well established technique able to discriminate different molecules through fluorescent decay lifetime. The potential of FLIM imaging, using the inherent fluorescence lifetime of the probes over the fluorescence intensity, is well known in the field of optical microscopy, including applications for tissue and clinical use [8–10]

Fluorescence species with distinct lifetimes, typically ranging from 1-10 ns, can be distinguished independent of their emission wavelength. When combined with multi-color spectral imaging, FLIM provides an additional selection process, increasing the number of distinct imaging channels. Furthermore, FLIM is generally insensitive to intensity variations or fluorophore density, making it a robust modality for distinguishing subtle changes. However, a major limitation is imaging speed. FLIM typically requires scanning methods to accommodate complex time-tagged single photon counting detection, and significant photon counts to construct meaningful lifetime histograms at each image pixel.

Fluorescence lifetime imaging endomicroscopy through an imaging fiber bundle has previously been demonstrated, although limited to imaging speeds around 10 seconds per frame. Kennedy et al. [11] used a 30,000 core coherent imaging fiber and were able to measure lifetimes down to 89 ps but with an acquisition time between 10 and 100 seconds per image frame. Bec et al. demonstrated a system [12] composed of a single scanning fiber with a moving probe able to record at a 30 Hz rate but requiring 500 images to produce the results shown in the paper, equivalent to 16 seconds acquisition per frame. Yankelevich et al. [13] used a single scanning fiber, to obtain sub-nanosecond precision lifetime but with an acquisition time of 9.8 seconds per frame.

In all cases the advantage of FLIM over conventional imaging is primarily dependent on the

ability to distinguish separate fluorescence lifetimes, the sensitivity of which is dependent on photon counts, the number of channels in the decay and fitting algorithms. Time-correlated single photon counting (TCSPC) is the most accurate technique for reproducing the true decay times [14], but is inherently slow, typically delivering a single image frame in 10s of seconds.

A system that could potentially deliver higher frame rate in endomicroscopy is described by Poland et al [15]. Their system is a confocal microscope that uses a "Megaframe" camera (MF32) based on a 32×32 SPAD array developed by the University of Edinburgh and STMicroelectronics [16, 17]. The SPAD array has a very low fill factor (1%) however, a spatial light modulator (SLM) synthesizes 8×8 beamlets that are scanned across the sample, before the resulting fluorescence is descanned and directed onto an 8×8 selection of the SPAD array with near 100% fill factor. The resulting 256×256 pixel images were recorded at 10 seconds per frame. However, the speed of acquisition remains limited and the use of the spatial light modulator complicates the optical setup rendering a potential clinical instrument bulky, due to the use of a Ti-Sapphire laser, and in need of complex alignment procedures.

In this paper we present an alternative approach that uses an entire MF32 SPAD array as a single, parallel SPAD detector, to reduce detection dead time and increase count rate and thus frame rate. We demonstrate 4-channel, one frame per second fluorescence imaging through a combination of dual channel FLIM and dual color, temporally dephased photon counting. We demonstrate the clinical potential of the endomicroscope by imaging *ex vivo* human lung with labelled *E.coli* bacteria compared to healthy lung.

2. Description of the instrument

A schematic of the multiplexed endomicroscope is shown in Figure 1. Two picosecond-pulsed laser sources (480 and 640 nm, Picoquant GmbH Germany) are driven at a repetition rate of 10 MHz. The trigger output of the 640 nm laser source drives the 480 nm source through an analog and programmable delay box, additionally triggering the MF32 camera to start the TCSPC acquisition. The two spectrally distinct fluorescence signals from green and red excitation are thus separated in time through this temporal offsetting of the two excitation lasers. The two laser sources are fiber coupled into two collimators, whose output are combined via a dichroic (FF506-DI03-25X36, Semrock USA) before passing through a 10 nm band-pass laser filter to clean the laser emission. The resulting beam is then scanned using a pair of close coupled galvos (ThorLabs Inc, USA).

The resulting scanned beam is conveyed through a CLS-SL visible scan lens (400–750 nm, Thorlabs, EFL 70 mm) and an ITL200 infinity-corrected tube lens (Thorlabs, f 200 mm), to a Nikon plan fluorite imaging objective, $\times 10$, 0.3 NA, that focuses the excitation light onto a multi-core fiber. The fiber has 30,000 cores, with sizes varying from 5-10 microns (Fujikura, Japan). The laser scan system is achromatic for the two excitation wavelengths but the imaging fiber is not. To mitigate this the system is aligned such that coupling is equally compromised for both excitation wavelengths.

The fluorescence is collected back from the distal end of the fiber bundle and the returning light is collected by the objective and passes back through the optical system to be descanned, before being transmitted by the dichroic filter and passing through a pass-band filter to ensure no laser light enters the M43L01, 105 μm 0.22 NA, multimode fibre that acts also as an optical pinhole before the detectors. The fluorescence signal, the output of the multimode fiber, can be switched to either an APD detector for 10 FPS fluorescence intensity images, or defocused to fill the MF32 camera for 1 FPS FLIM imaging.

The non-resonant scanning galvos are driven to achieve one frame per second imaging rate in a raster scan mode. However, by using a spiral pattern we were able to obtain frame rates in excess of 10 FPS in fluorescence imaging mode. When in the spiral scanning mode the scan matches the circular fiber bundle closely. An important advantage of using non-resonant galvos

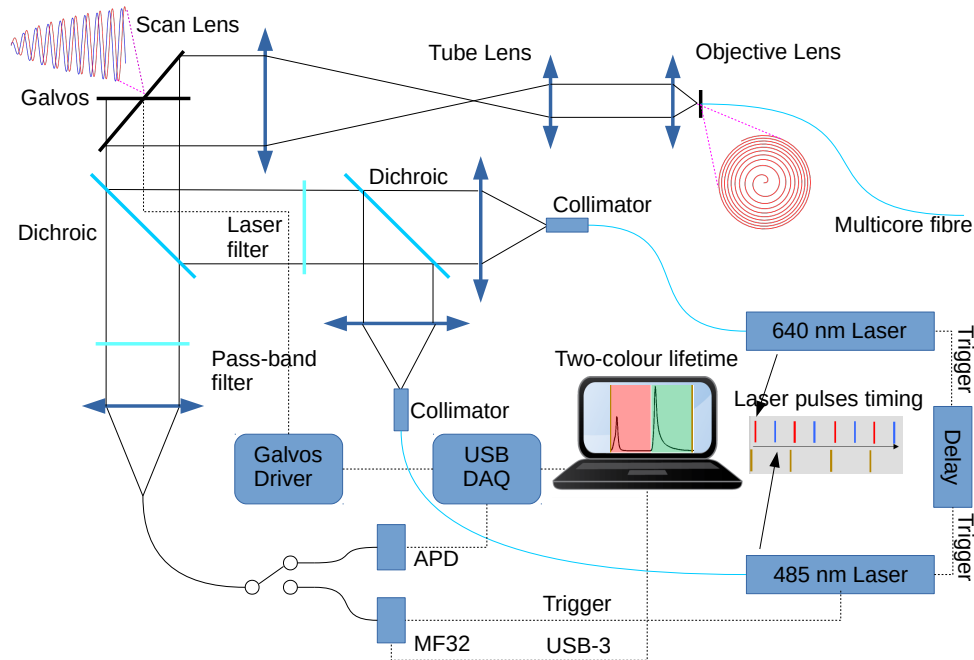


Fig. 1: Optics diagram and block diagram of the laser scanning endomicroscope. A USB controlled DAQ generates the scanning waveforms and acquires the analog signal from the APD when in pure intensity scanning mode. The MF32 camera for FLIM data acquisition is controlled through a separate USB interface. Bottom right shows the trigger signal path originating in the 640 nm laser, passing through a delay box, triggering the 485 nm laser and finally triggering the MF32 camera. The emission, dichroic and excitation filters are the XF454 set from Horiba. The schematic shows a raw histogram as acquired from the MF32 camera, showing the red fluorescence decay and the temporally shifted green fluorescent decay

is that they allow us to freely control scan rates, patterns and ranges (e.g. Figure 2). For example, the architecture described here is appropriate for performing wide field of view imaging, for focusing on specific targeted areas of tissue or for addressing single fibre cores.

To demonstrate the basic performance of the system, Figure 2 shows a 1951 USAF resolution test chart coated on the underside with an ultra-high density of fluorescent microspheres, imaged in fluorescent mode using the APD. The sequence starts with a high-resolution image of group 7, element 2 of the chart, where the single cores of the fiber are visible and zooms out to a larger field of view. Optical resolution is limited by both core spacing (around $5 \mu\text{m}$) and by core to core coupling [18].

In FLIM modality the system uses the MegaFrame 32×32 SPAD array as a single-pixel detector, rendering the detection from the 1024 individual SPAD detectors parallel. In the low photon detection limit employed here, incident photons stochastically impact on each pixel in the array and the signals from each of the 1024 SPADs detectors are then binned in a single temporal histogram of the photon arrival time for each single frame from the SPAD array producing the signal of a single pixel in the final image. Crucially this parallelization increases the maximum

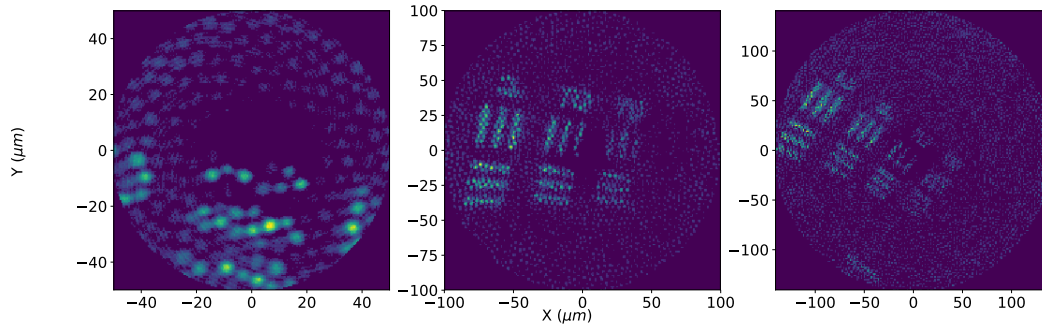


Fig. 2: Fluorescent image sequence acquired in non time-resolved mode of a 1951 USAF resolution test chart. The sequence starts left with the highest resolution and ends right with lower resolution, zooming out of group 7, element 2. The single cores of the imaging fibre ($5\ \mu\text{m}$) are visible in the highest resolution image.

detectable number of photons per unit time enabling more efficient use of the fluorescently excited photons with a high counting rate. It has previously been demonstrated [19], that the use of a 8×8 SPAD array, as a single-pixel detector, showed a factor 64 increase in photon rate.

In this system operation, photon counts per detector are below the maximum detector readout rate of hundreds of kHz [17] (total count rate increased to hundreds of MHz by detector parallelization over the whole array), while laser repetition rate is 10 MHz. If an imagined (the authors are not aware of such a device) single detector capable of 100 MHz photon count rates were used (equivalent to the maximum count rates possible here), and operated near these rates then photon pileup [20] would be overwhelming. Even at two orders of magnitude lower rates (MHz) pileup would cause perturbation of the observed photon timing statistics. This would lead to shortened observed fluorescence lifetimes, and variations of this artifact with varying numbers of photon counts. Meanwhile, at the 100 MHz maximum possible count rates in our system each detector is operating at only 1.0% of the laser repetition rate, a regime recognized to be safe from photon pileup [20].

The red and green photons reaching the detectors of the MF32 camera are separated in time due to the delay introduced in triggering the blue laser with respect to the red laser, this delay being much longer than any of the fluorescence lifetimes, as shown in Figure 1. Counts in one color do not have an effect on the other channel (due to photon pileup) in the noted regime where counts are low per detector compared to laser repetition rate. Only in such a parallel detection scheme is high speed FLIM not in danger of photon pileup artifacts, and temporal color multiplexing becomes viable as described.

Histogramming the photon counts across all parallel pixels of our detector also combines the dark counts present. Statistical noise in a measurement is dependent on the square root of the counts. As such, parallelization which simultaneously increases both photon counts and dark counts results in less noisy counting statistics than those of a count rate limited system.

For fast lifetime imaging we use a center of mass (C-O-M) algorithm [15] for real time calculation of the exponential lifetime for both the green (485 nm excitation) and red (640 nm excitation) fluorescence. As in standard beam scanned FLIM, the photon counting occurs for a fixed dwell time for each scanned point, building up a complete image during the scan. Raw data was saved as flexible image transport system (FITS) format [21] as a sequence of 32×32 images from the MF32 with the associated scanner position enabling multiple alternative methods suitable for processing to obtain fully fitted TCSPC FLIM images. The system scan speed is limited to one frame per second by the SPAD array to FPGA transfer speed.

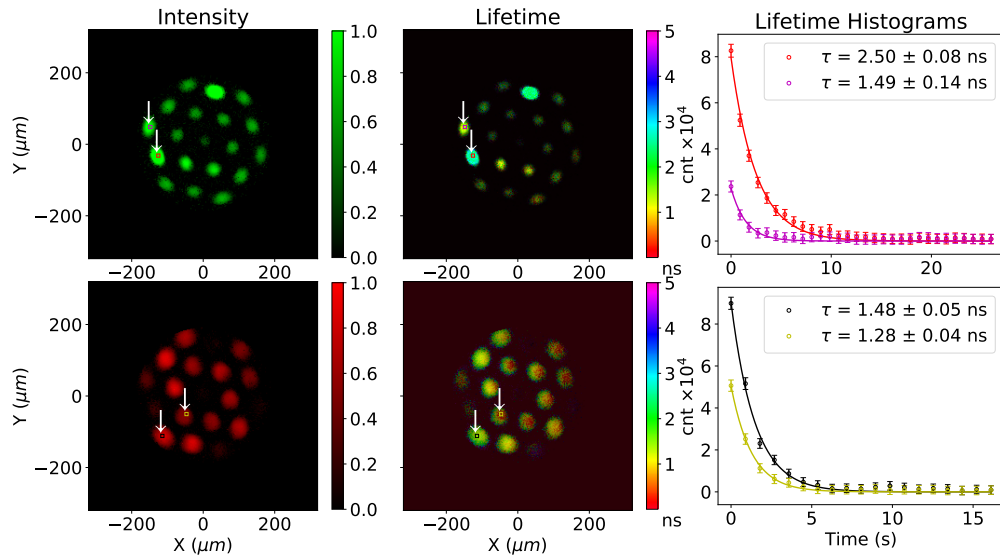


Fig. 3: A multi-core fiber loaded with four different fluorescent microspheres acquired at 1 FPS. Top shows the green channel and bottom the red channel. The left hand column shows a fluorescence image, the center column a lifetime image. The plots show the lifetime measured from two distinct areas of 9×9 elements in the figures, marked by red and purple squares on the top row and black and yellow squares on the bottom row. The plots and the uncertainties were obtained using a single exponential fit with the `scipy.optimize.leastsq` module [22]. The FLIM images use the center-of-mass method [15].

3. Results

We demonstrate the potential of the instrument by first using an example system of a multi-core fiber with 19 widely spaced cores with the distal end loaded with fluorescent microspheres, then utilizing a 30,000-core imaging fiber to view microspheres on a slide, and then viewing *ex vivo* human lung-tissue to show the detection of bacteria against a strong spectrally similar fluorescence background using lifetime as the contrast mechanism. Images were obtained in 10-FPS fluorescence mode and in 1-FPS FLIM mode, in single and dual color modalities.

3.1. FLIM capability test with fluorescent microspheres

To demonstrate the basic operation of the system a loaded fiber was used in place of the normal imaging fiber. Four types of microspheres were loaded on to the distal end of a 19-core multimode fiber with $10 \mu\text{m}$ cores. Pits $10 \mu\text{m}$ in diameter were formed by selectively etching the cores using hydrofluoric acid, into which microspheres self-locate. This configuration is used for sensing pH and other physical parameters, using procedures described in [23,24]. Two types of microspheres had “red” emission, two with “green” emission and each with different lifetimes. Specifically we used $10 \mu\text{m}$ silica microspheres covalently bound to Fluorescein (green), TAMRA (orange), NBD (yellow) and CY5 (red) dyes. The Results are shown in Figure 3.

Figure 3 shows in the top panels the green channel and the bottom panels the red channel. On the left side intensity images are shown while in the center lifetime images are shown. The right side of Figure 3 shows the average histogram of the photon arrival time from the two red and purple square areas drawn on the intensity and FLIM images.

We find that the resulting histogram obtained for each scanned point is more than adequate

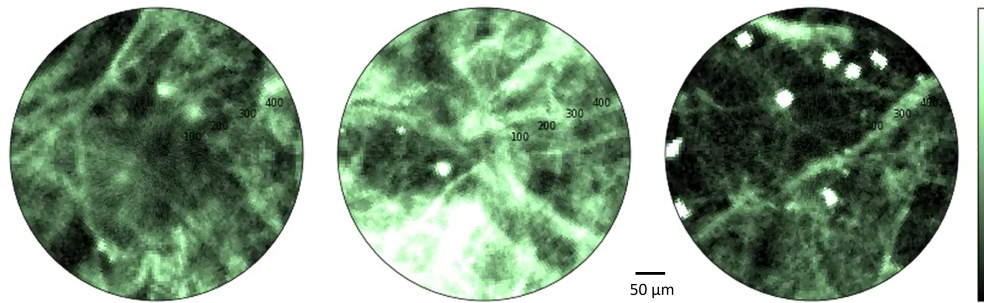


Fig. 4: Above are three frames extracted from a 10 FPS movie from *ex vivo* lung tissue taken in in non time-resolved modality using the APD detector. Some monocyte cells labeled with Calcein are visible in the foreground. The image intensity represents the voltage output of the APD (in response to fluorescence intensity) on the indicated color scale. The field of view is 500 μm . Parameters were kept constant throughout the image frames giving good contrast of lung tissue, however some saturation of brighter features is therefore present.

to produce FLIM images at the rate of one FPS. The histograms of Figure 3 each show two exponential decays for the same wavelength of emission from the two lifetimes for the microspheres present. The green channel in the top plots shows two distinct lifetime species, 1.51 ns and 2.56 ns. The red channel also shows two distinct lifetime species, 1.47 ns and 1.29 ns. Distinction of these species is subjective in the intensity only images, but quantifiable in the lifetime images. Thus our system can easily distinguish 4 distinct species, through both spectral and temporal identification. Temporal accuracy is limited by the laser pulse width, which is approximately 100 ps [16]. This result demonstrates the ability to resolve signals from four different probes through multi-spectral FLIM at 1 FPS.

The lifetime images were weighted by the fluorescent images so that low signal-to-noise (SNR) pixels are not shown. Weighting was done by modulating the alpha channel, which controls the transparency of the image, of each FLIM image with the fluorescent image. In this way low SNR pixels become transparent and disappear from the image, but the weighting does not impinge on the color scale for the lifetimes as traditional intensity weighting would.

To demonstrate high speed FLIM we include frames from dynamic measurements in the Appendix. Figure 7 shows 8 extracted frames from a 1-FPS movie, imaged under similar conditions as described for Figure 3 but utilizing the imaging fibre. The sample consisted of mixed red and green fluorescent microspheres of the same type as described in the previous experiments. They were deposited on a microscope slide as a liquid solution and let dry. The 30,000 core imaging fibre was put nearly in contact with the slide and shifted manually using a translation stage. The microspheres in Figure 7 are seen shifting from right to left. Each row represents a single temporal frame. Frame one is at the top. The columns from the left show a green fluorescent image, a green lifetime image, a red fluorescent image and a red lifetime image. Figure 8 shows an additional movie. We used the same sample as in Figure 3. This time the fibre probe with fluorescent microspheres were placed in water during the capture. The red microspheres show a decrease in lifetime from 1.8 ns to about 1.2 ns after water was added. The green microspheres show a decrease of lifetime from 0.9 ns to about 0.1 ns while additional green microspheres show a decrease from 2.4 ns to 1.6 ns.

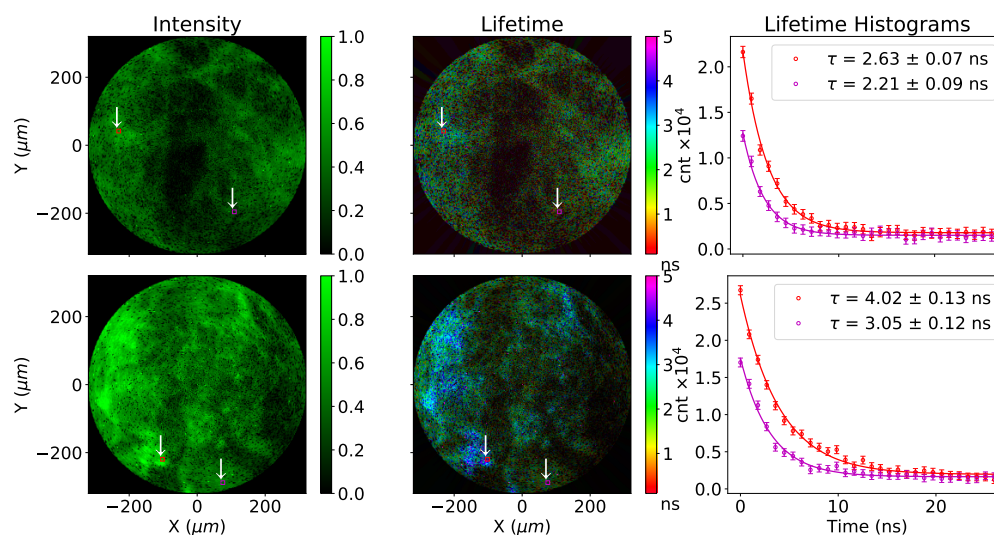


Fig. 5: *Ex vivo* human lung tissue. The top row shows human lung and bottom row shows human lung plus *E.coli* and NBD-PMX smartprobe. The rightmost plots show the lifetime measured from two distinct 9×9 element areas in the figures, represented by a red and a purple squares.

3.2. *Ex vivo* human lung tissue imaging with labeled bacteria

To demonstrate the clinical significance of the instrument experiments were undertaken on *ex vivo* human lung samples artificially infected with labeled bacteria. Human lung samples were obtained from patients undergoing surgical resection for lung carcinoma. All lung sections used in this study were sections of normal healthy lung away from the cancerous growth. The study was approved by the Regional Ethics Committee (REC), NHS Lothian (reference 15/ES/0094), and with informed consent of the patients. Human lung tissue samples were dissected into thin, small sections (4 mm by 4 mm) and placed onto a 96-well tissue culture plate for imaging.

Figure 4 shows an extract from a 10 FPS intensity only movie of *ex vivo* lung populated with live fluorescent monocyte cells of approximately ($9 \mu\text{m}$) and labeled with Calcein. (see supplementary Movie S1 for full video) The movie was acquired using the APD single pixel detector. As discussed previously, human lung is naturally autofluorescent in the green mainly due to the presence of elastin and collagen in the connective tissue therefore Calcein provides contrast by making the monocyte cells brighter. Functioning in this conventional modality the system demonstrates the observation of lung structures at 10 FPS through fibre, but it is clear that weak signals from fluorophores could be obscured by the lung autofluorescence.

3.3. Human lung with NBD-PMX bacterial imaging smartprobe

Overnight cultures of *E.Coli* grown in LB broth (250 rpm, 37°C) were washed (x3) in phosphate buffered saline (PBS, Gibco) and then adjusted to an OD_{595} of 2. The bacteria were labeled with a NBD-PMX smartprobe [6, 7] at $5\mu\text{M}$ concentration and were washed in PBS to remove any excess dye after approximately 1 minute. For imaging, pre-labelled *E. Coli* ($100\mu\text{L}$) were added to a section of lung tissue in a 96-well tissue culture plate and imaged immediately.

Figure 5 (top) shows *ex vivo* human lung tissue imaged in lifetime mode with the MF32 and C-O-M analysis described previously. Healthy lung tissue (top) and that artificially infected with *E.coli* labelled with a NBD-PMX smartprobe (bottom) are shown. The left images show intensity only, taken from summing photon counts from the FLIM data, and the right images the

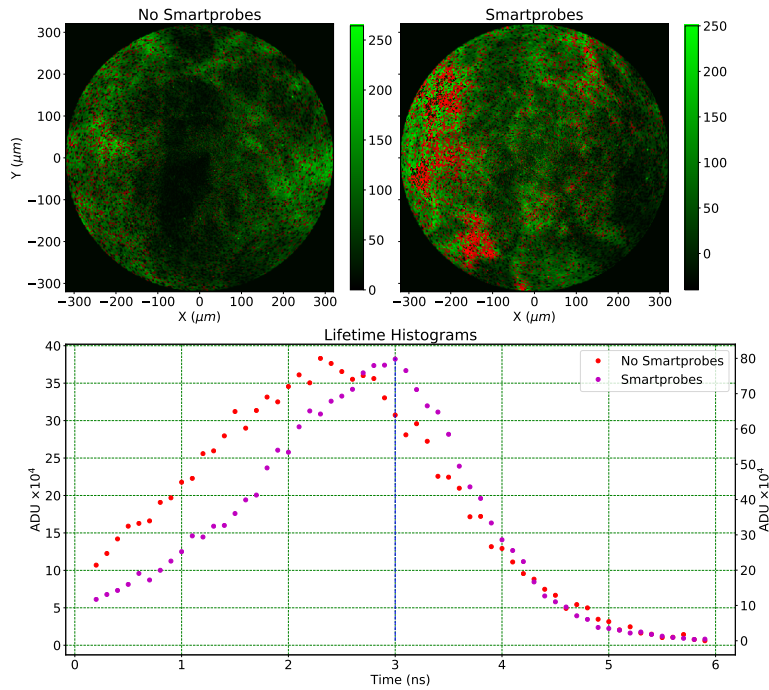


Fig. 6: Top left is *ex vivo* lung and top right is *ex vivo* lung with NBD-PMX smartprobe labeled bacteria. The bottom panel shows two histograms of the lifetime distribution from the whole images. The red histogram is from the left image without smartprobes and the purple histogram from the right image with smartprobes. A threshold of 3 ns was applied to the FLIM data to identify regions where the smartprobes were active. The red dots on the right image represent the region where lifetime was larger than 3 ns and counts were larger than 50.

intensity weighted FLIM images. All images were recorded at a rate of 1 FPS, but here 10 static frames have been combined to provide a clearer image. The rightmost plots show the average histogram of the photon arrival times from the two red and purple squares on the fluorescent and FLIM images. The intensity only images show a characteristic increase in intensity for the infected tissue, but identification of the smart probe labeled bacteria is challenging over the spectrally overlapping autofluorescence. In lifetime mode the distinction between bacteria (with lifetime 4.0 ns) and autofluorescence (lifetime 3.0 ns) is much clearer. Thus lifetime here acts as an excellent contrast mechanism [7].

To further exemplify this distinction, Figure 6 shows the same data from Figure 5 with temporal thresholding applied using the histograms from the lifetime of the two images to determine the threshold. The top panel reproduces the FLIM image with and without smartprobe labeled bacteria, the bottom panel shows a binned histogram of each image. A 3 ns threshold, corresponding to the peak of lifetimes in the smart probe labeled data, was applied to the top images and the resulting pixels with lifetime above this threshold are then colored red and shown in both images of Figure 6 but only notable in the right figure when smart probe labeled bacteria were present. With this example of thresholding, tuned to the smartprobe lifetime, the smartprobes become immediately visible in the FLIM image while being hidden in the fluorescent image.

This result demonstrates the clear potential for distinguishing fluorescently labelled bacteria from the intrinsic auto-fluorescence of lung tissue, based on lifetime through an imaging fiber

at one frame per second with simple, real time enabled processing algorithms. This method is appropriate for *in vivo* clinical use, where it is not normally possible to spectrally separate the smartprobe from lung autofluorescence [6].

4. Conclusions

We have developed and built a dual-color, FLIM enabled laser scanning endomicroscope capable of fluorescence lifetime imaging endomicroscopy at one frame per second. The system uses a Megaframe 32×32 SPAD array detector as a single-pixel detector, with all 1024 detectors contributing to the buildup of a histogram per scanned image element.

A center-of-mass algorithm with background subtraction was then used to determine the lifetime. We obtained FLIM images at a rate of one frame per second and show standard fluorescence imaging at a frame rate of 10 FPS with non-resonant galvos, using a spiral scan pattern rather than the more conventional raster scan. This enables a more flexible endomicroscopy system, capable of selecting regions of interest with controllable zoom, scan range and scan rate.

We have shown that the endomicroscope is capable of dual-colour imaging by separating the green and red channel in time using our high speed fast recovery detector. We have also shown that each single color channel can discriminate microspheres of different lifetime. We detected *E.coli* bacteria in *ex vivo* human lung using a fluorescent NBD-PMX bacterial imaging smartprobe [6] that provides longer lifetime in FLIM imaging (4.02 ± 0.13 ns) from a lung background of 2 to 3-ns. This demonstrates that using integrated SPAD arrays and lifetime imaging it is possible to use fluorescence lifetime as a contrast mechanism to help remove background auto-fluorescence in human tissue. The method is suitable for clinical use with a current imaging frame rate of 1 frame per second currently limited by the data transfer speeds.

Funding

We thank the Engineering and Physical Sciences Research Council (EPSRC, United Kingdom) Interdisciplinary Research Collaboration grant EP/K03197X/1 for funding this work.

Acknowledgments

This research has made use of NASA's Astrophysics Data System Bibliographic Services. This research made use of IPython [25]; Matplotlib, a Python library for publication quality graphics [26]; SciPy [22], a Python library for scientific computing; Cython [27], a Python library for C/C++ code wrapping.

Disclosures

The authors declare that there are no conflicts of interest related to this article.

5. Appendix

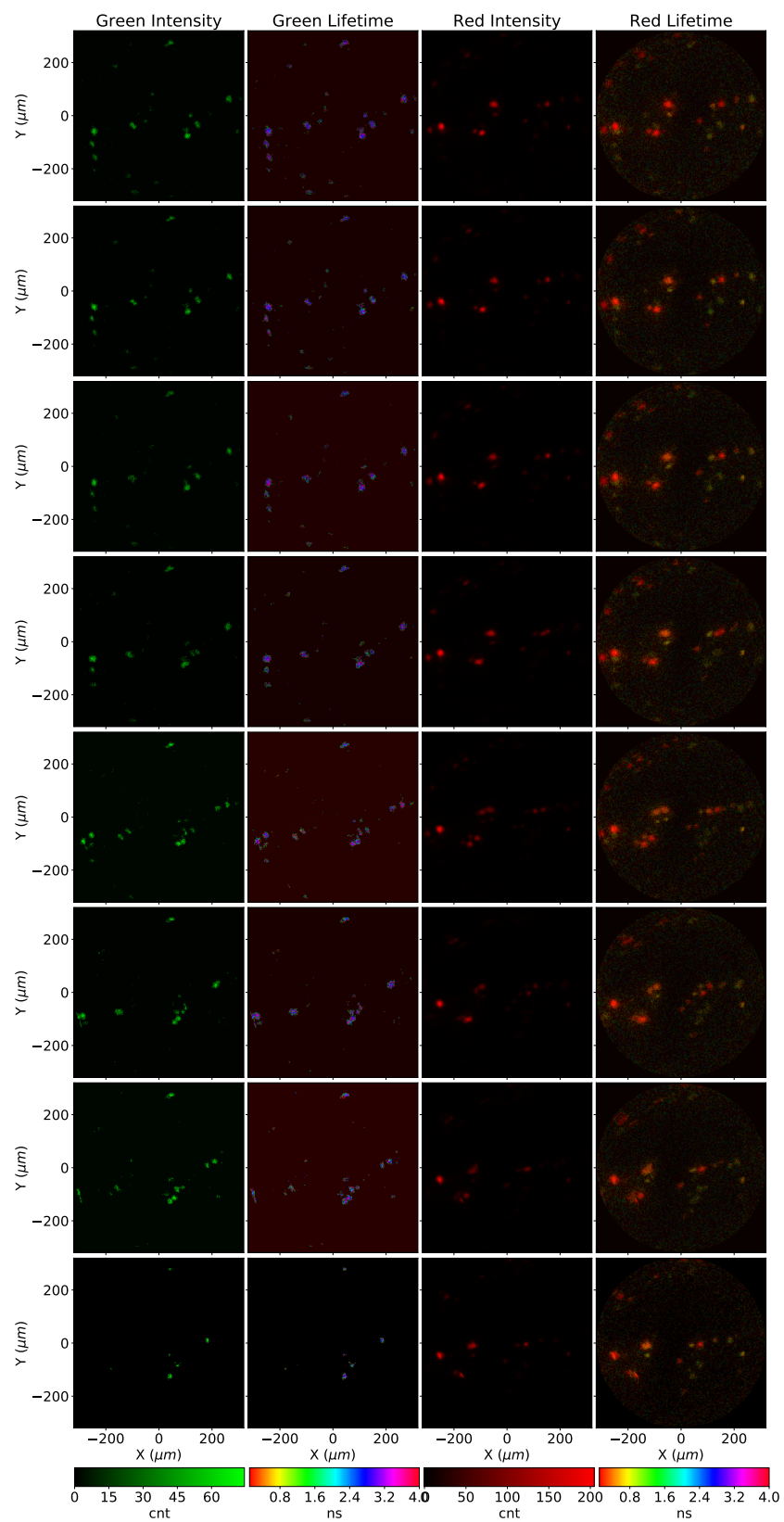


Fig. 7: Sequence of eight images extracted from a ten-frames, 1-FPS FLIM movie. Microspheres covalently bound to Fluorescein (green), TAMRA (orange), NBD (yellow) and CY5 (red) dyes were deposited in a microscope slide. The imaging fiber was mounted on a XYZ translation stage and moved a few μm across the surface of the slide.

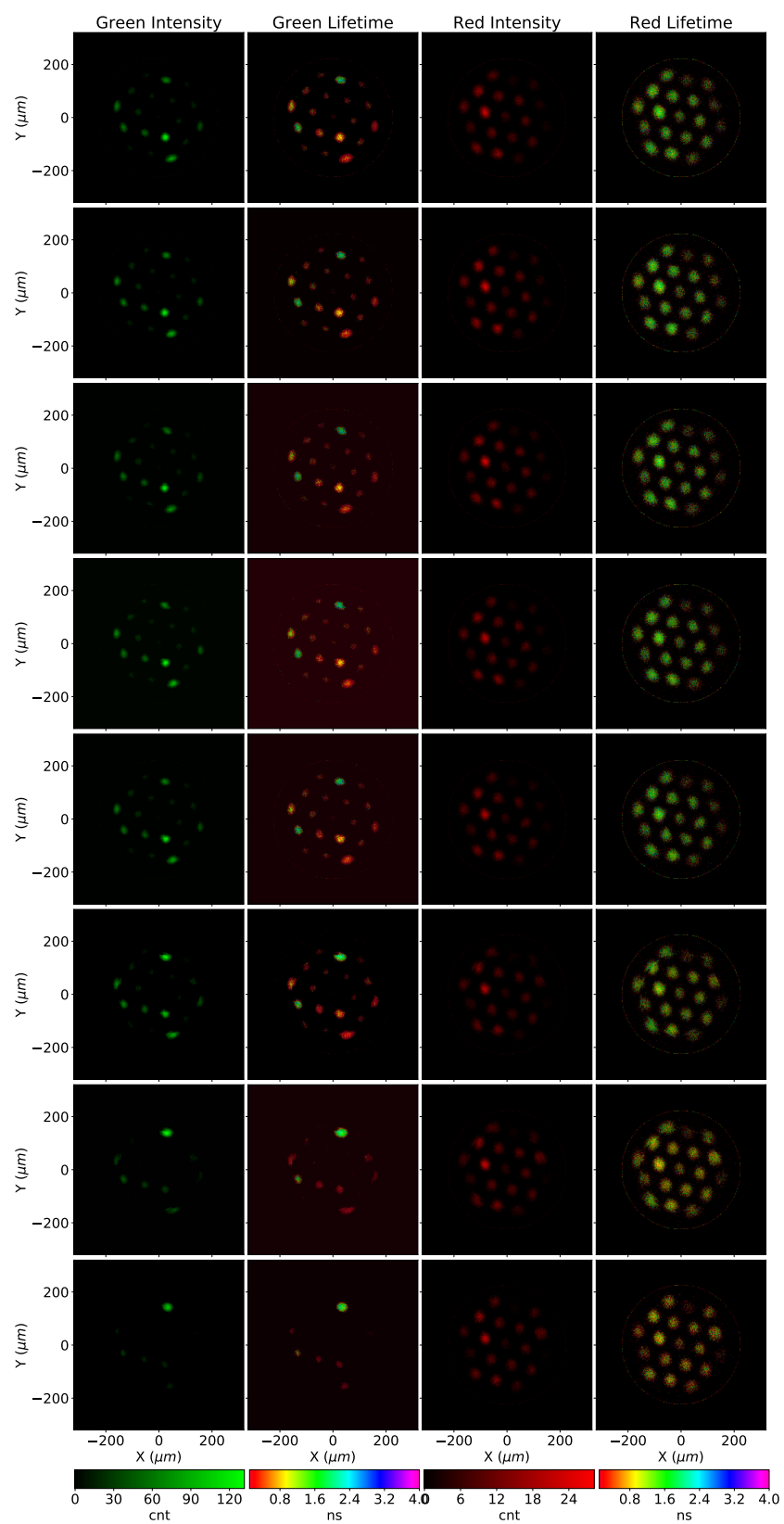


Fig. 8: Sequence of eight images extracted from a ten-frames, 1-FPS FLIM movie. Microspheres covalently bound to Fluorescein (green), TAMRA (orange), NBD (yellow) and CY5 (red) dyes were loaded onto a multi-core fiber. The fiber was placed in water during recording, causing most microspheres to show a decrease in lifetime.